Adaptive Observer for Sensorless Control of Stand--Alone Doubly Fed Induction Generator

Journal:	*Transactions on Industrial Electronics*
Manuscript ID:	draft
Manuscript Type:	SS on Application and Control of Doubly Fed Induction Machnines
Manuscript Subject:	Renewable Energy Systems
Keywords:	Induction generators, Observers, Generators
Are any of authors	Yes

IEEE Member?:	
Are any of authors IES Member?:	Yes

Adaptive Observer for Sensorless Control of Stand–Alone Doubly Fed Induction Generator

Post ISIE2008 Paper

***Abstract*— A control strategy for a Doubly–Fed (wound rotor) Induction Machine working in variable-speed stand-alone power system without using mechanical sensors is presented in this paper. Stator voltage magnitude and frequency are regulated using two control loops based on field orientation theory. A Luenberger observer is used to estimate the stator flux, while an adaptive scheme modifies the rotor position required in the stator flux estimation. The proposed controls behaves very well in steady state as well as transient states like: start–up, varying speed or electric load changes. Experimental results are presented to validate this proposal.**

I. Introduction

The Doubly–Fed Induction Machine (**DFIM**) is one of the most used machine in generation system connected to the grid or working in stand–alone mode. The main advantage of the DFIM working in stand–alone generation system with variable (restricted) speed, is the reduced size of the power electronic converter needed on the rotor side [1], [2]. This makes the generation system suitable for variable speed diesel hydro– and wind–energy turbine applications.

Stand–alone systems must be able to provide the users with regulated voltage and frequency [3]. In these cases, the DFIM presents several advantageous characteristics [4]. Stator voltage and frequency regulation can be achieved using two back–to–back converters connected to rotor windings (Rotor Converter, **RC**) and stator windings (Front End Converter, **FEC**) as can be seen on Fig. 1. RC is used to control the rotor currents in order to obtain the desired stator voltage and frequency control of DFIM. FEC can be controlled to regulate DC-Link voltage and filter harmonic currents introduced by non–linear loads connected to the system [5], [6].

Most DFIM control strategies requires the rotor position knowledge to achieve the orientation of rotor currents. Usually a position sensor like a shaft encoder is employed. The elimination of this sensor decreases size, costs, cabling and maintenance of the drive. It also increases the system reliability and noise immunity. So sensorless schemes appear to be very attractive and have been in constant evolution in the last years. Sensorless strategies usually does an estimation of the machine flux using some kind of observer. Several proposed observers are open loop estimators in the sense that they have no error correction mechanism. This kind of estimators are not able of either modifying their convergence speed or ensure stable convergence under parameter uncertainties or measurement noise [7]–[9].

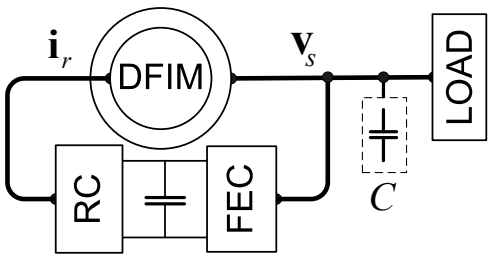

Fig. 1. Stand–alone variable–speed generation system.

Classical Model Reference Adaptive Systems (**MRAS**) approach compares the reference model output with the adaptive model outputs to obtain the estimation error used by the adaptive law to achieve the convergence of the adaptive model to the reference model [10], [11]. Using this kind of observer the convergence of the adaptive model to the reference model can be ensured, although, the reference model must be an exact description of the actual system. Other MRAS approaches uses the actual system measurements as the reference model outputs avoiding reference model errors. This kind of systems compares the adaptive model output with real system output measurements to obtain an estimation error used by the adaptive law [12], [13].

Other authors have proposed Adaptive Luenberger observers to estimate some machine parameters and rotor speed for the induction machine used as motor [14]–[16]. This kind of observer have shown better performance than others when used on induction motor applications [17].

In this paper, a control strategy to regulate the frequency and voltage of a DFIM working as a variable speed stand–alone generating system is proposed. An Adaptive Luenberger observer has been proposed to estimate stator flux and rotor position in [18]. In that paper, simulation results were presented to test the behavior of the control loops and observer under load and speed changes, as well as parameters mismatch. In this paper experimental results are introduced. They validate the performance of the proposed control.

In detail the paper is organized as follows: the DFIM model is presented in Section II-A. The field oriented control loops developed to regulate stator voltage magnitude and frequency are presented in Sections II-B and II-C. An Adaptive Luenberger observer to estimate stator flux and rotor position is presented in Section III. The observer behavior is evaluated through simulations which are shown in Section IV. The complete system performance is evaluated through experimental results which are shown in Section V. Finally, conclusions are given in Section VI.

II. DFIM Control

The main goal of the control strategy presented is to implement a stand–alone generation system providing regulated stator voltage magnitude and frequency using a DFIM without a position sensor. Two independent control loops are designed to regulate stator voltage magnitude and frequency.

The frequency control loop is realized aligning the stator flux with a reference frame rotating with synchronous speed. This strategy for frequency control is preferred since the estimated flux offers smother signals than the measured voltages. On the other hand, the voltage magnitude is directly controlled using a PI control loop built-up using the stator voltage measurements.

A. DFIM model

The DFIM can be described by the following equation using a reference frame rotating at arbitrary speed ω_{dq} [19],

$$\dot{\boldsymbol{\lambda}}_s = \omega_{dq}\,\mathbf{J}\,\boldsymbol{\lambda}_s - r_s\,\mathbf{i}_s + \mathbf{v}_s, \tag{1}$$

where r_s, is the stator resistance, $\boldsymbol{\lambda}_s$, $\mathbf{v}_s$ and $\mathbf{i}_s$ are the stator flux, stator voltage and current vectors referred to an arbitrary reference frame respectively and

$$\boldsymbol{\lambda}_s = \begin{bmatrix} \lambda_{qs} \\ \lambda_{ds} \end{bmatrix}, \mathbf{v}_s = \begin{bmatrix} v_{qs} \\ v_{ds} \end{bmatrix}, \mathbf{i}_s = \begin{bmatrix} i_{qs} \\ i_{ds} \end{bmatrix}, \mathbf{J} = \begin{bmatrix} 0 & -1 \\ 1 & 0 \end{bmatrix}.$$

For the present work, ω_{dq} is considered equal to the desired stator frequency ($50\ [Hz]$) so the arbitrary reference frame becomes the desired synchronous one. The stator flux can also be obtained from stator and rotor currents like

$$\boldsymbol{\lambda}_s = L_s\,\mathbf{i}_s + M\,\mathbf{i}_r, \tag{2}$$

where L_s is the stator inductance, M is the magnetizing inductance and $\mathbf{i}_r$ ($\mathbf{i}_r = [i_{qr}, i_{dr}]^T$) is the rotor current referred to the synchronous reference frame. This stator flux current model can also be expressed as follows

$$\boldsymbol{\lambda}_s = L_s\,\mathbf{i}_s + M\,e^{j(\theta_r - \theta_{dq})}\,\mathbf{i}_r^r, \tag{3}$$

where θ_r is the rotor position defined as the angular displacement between the rotor and stator circuits, θ_{dq} is the angular position of the synchronous reference frame and $\mathbf{i}_r^r$ ($\mathbf{i}_r^r = \left[i_{qr}^r, i_{dr}^r\right]^T$) is the rotor current referred to a reference frame fixed to the rotor. This is the rotor current which can be directly measured.

B. Stator Frequency control loop

The angular speed of the stator flux space vector must be constant in order to generate a stator voltage constant frequency. The frequency control is achieved by defining a synchronous reference-frame and forcing the stator flux vector to be aligned with its d-axis, so that,

$$\lambda_{qs} = 0 \qquad \text{and} \qquad \dot{\lambda}_{qs} = 0. \tag{4}$$

The frequency control loop is implemented using a PI controller with q–component flux reference defined as $\lambda_{qs}^* \equiv 0$. The q-component stator flux estimate $\hat{\lambda}_{qs}$ obtained from the stator flux observer proposed in Section III is used to calculate the rotor current q-component (i_{qr}^*), used as the actuation variable,

$$e_{\lambda_{qs}} = -\hat{\lambda}_{qs}, \tag{5}$$

$$i_{qr}^* = K_{Pf}\,e_{\lambda_{qs}} + K_{If}\int e_{\lambda_{qs}}\,dt. \tag{6}$$

This control loop is presented in the lower part of the block diagram shown on Fig. 2. The frequency control loop bandwidth should satisfy a trade–off between load perturbation rejection and the measurement noise rejection capabilities.

The angular position of the reference frame (θ_{dq}), is obtained from a free–running integral as follows,

$$\theta_{dq} = \int \omega_{dq}\,dt. \tag{7}$$

θ_{dq} is used to transform and anti–transform currents and voltages as shown in Fig. 2.

C. Stator Voltage Magnitude control loop

The stator voltage magnitude control loop is designed to regulate the voltage magnitude (V) of the DFIM stator voltage vector, defined as follows,

$$V = \sqrt{v_{qs}^2 + v_{ds}^2}, \tag{8}$$

where v_{qs} and v_{ds} are the quadrature and direct axis components referred to a synchronous reference frame.

The stator voltage control loop is implemented using a PI controller where the voltage error (e_{V_s}) can be defined as

$$e_{V_s} = V^* - V. \tag{9}$$

The main goal of this control loop is to reject the voltage variations produced by electric load or speed changes.

The d–component of the rotor current (i_{dr}) modifies the d–component of the stator flux which also modifies the stator voltages as can be deduced from (1) and (2). Then this current is used as the actuation variable for the stator voltage control loop, so,

$$i_{dr}^* = K_{Pv}\,e_{V_s} + K_{Iv}\int e_{V_s}\,dt. \tag{10}$$

The stator voltage magnitude control loop is presented in the upper part of the simplified block diagram shown on Fig. 2.

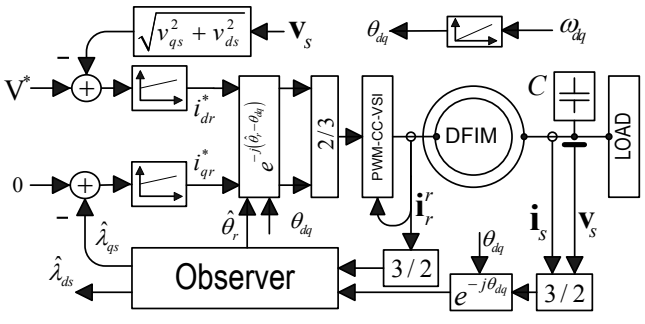

Fig. 2. Stator voltage magnitude and frequency control block diagram.

The band-width of this control loop should satisfy a trade–off between load perturbation and the measurement noise rejection capabilities.

III. Observer

An adaptive observer for estimating the stator flux and rotor position is proposed in this section. The stator flux estimation is obtained from a Luenberger observer.

The angular difference between the estimated and the measured rotor current vectors is used to build an adaptive law to estimate the rotor position. The correction term of the Luenberger observer is calculated using this rotor position estimation. Fig. 3 shows a block diagram of the proposed observer.

A. Stator Flux estimation

The stator flux is estimated using a Luenberger observer as follows

$$\dot{\hat{\boldsymbol{\lambda}}}_s = \omega_{dq}\,\mathbf{J}\,\hat{\boldsymbol{\lambda}}_s - r_s\,\mathbf{i}_s + \mathbf{v}_s - \mathbf{G}\left(\hat{\boldsymbol{\lambda}}_s - \boldsymbol{\lambda}_s\right), \quad (11)$$

where $\hat{\boldsymbol{\lambda}}_s$ is the stator flux estimate and $\mathbf{G}$ is the error correction matrix,

$$\mathbf{G} = \sigma\,\mathbf{I} - \omega_{dq}\,\mathbf{J}, \quad (12)$$

where σ is the observer gain. The design of the error correction matrix can be found in [20].

Using this kind of observer, the convergence transient of the estimation error ($e_{\lambda s} = \hat{\boldsymbol{\lambda}}_s - \boldsymbol{\lambda}_s$) is exponential and the observer gain is chosen to set the desired speed of convergence.

Since the actual stator flux cannot be measured, a good guess can be obtained using,

$$\boldsymbol{\lambda}_s = L_s\,\mathbf{i}_s + M\,e^{j\left(\hat{\theta}_r - \theta_{dq}\right)}\,\mathbf{i}_r^r, \quad (13)$$

where $\hat{\theta}_r$ is the rotor position estimation obtained as described in the next subsection.

B. Rotor Position estimation

First, an estimation of the rotor currents in a reference frame fixed to the rotor ($\hat{\mathbf{i}}_r^r$) is obtained using the stator flux estimation from (11) and (13),

$$\hat{\mathbf{i}}_r^r = e^{-j\left(\hat{\theta}_r - \theta_{dq}\right)}\left(\hat{\boldsymbol{\lambda}}_s - L_s\,\mathbf{i}_s\right)/M, \quad (14)$$

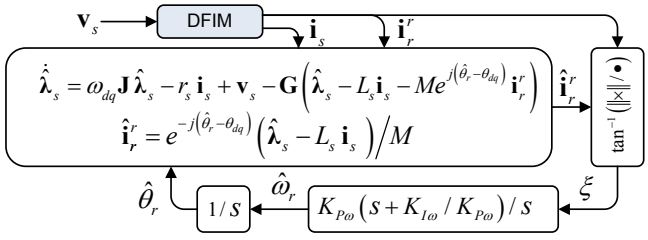

Fig. 3. Proposed observer simplified block diagram.

then, the rotor position can be estimated using the angular difference (ξ) between the estimated rotor current ($\hat{\mathbf{i}}_r^r$) and the measured rotor current ($\mathbf{i}_r^r$).

It is not simple to calculate the angular difference between two vectors when the vector angles are defined over a large range $(-\pi, \pi)$. Some proposed observers uses the cross product between two vectors ($\xi_\times = \hat{\lambda}_{\alpha s}\lambda_{\beta s} - \lambda_{\alpha s}\hat{\lambda}_{\beta s}$) as the error to estimate rotor position on induction machines [10], [11]. In these cases the error depends on the magnitude of the vectors to be aligned [12], [13]. Moreover, the cross product is a non–linear function of the angular difference (α) between both vectors ($\xi_\times \cong \sin(\alpha)$) which is less sensitive to big angular errors, as those above $\pi/2$.

This dependence can be avoided normalizing the cross product with the dot product of both vectors. In this way a better estimation for the angular error is calculated as,

$$\xi = \tan^{-1}\left(\left\|\hat{\mathbf{i}}_r^r \times \mathbf{i}_r^r\right\| / \left(\hat{\mathbf{i}}_r^r \cdot \mathbf{i}_r^r\right)\right) \quad (15)$$

Using (15) requires only one $\tan^{-1}$ (`atan2`) for solving angular difference and the programming algorithm becomes simpler and better defined than using the angular difference directly. Solving the angular difference directly require two $\tan^{-1}$ for solving individual angles and additional calculus must be performed to solve the result on a range of $(-\pi, \pi)$. Moreover, (15) offers a simple way of getting the required angular difference independently of the vector magnitude in the whole range.

Fig. 4 shows both error signals. It is clear that an angular difference near $\pm\pi$ radians means a value of $\xi_\times$ near zero when only the cross product is used.

This angular difference can be driven to zero using a PI controller as follows,

$$\hat{\omega}_r = K_{P\omega}\,\xi + K_{I\omega}\int \xi\,dt, \quad (16)$$

where $\hat{\omega}_r$ is the estimated rotor speed.

The rotor position estimation is obtained integrating $\hat{\omega}_r$,

$$\hat{\theta}_r = \int \hat{\omega}_r\,dt. \quad (17)$$

IV. Observer Performance

In order to test the proposed observer, simulations were carried out with SIMULINK/MATLAB. Here, the proposed control loops use the actual stator flux and rotor position as feedback signals. Simulations are preferred at this instance because the actual stator flux cannot be measured (without using

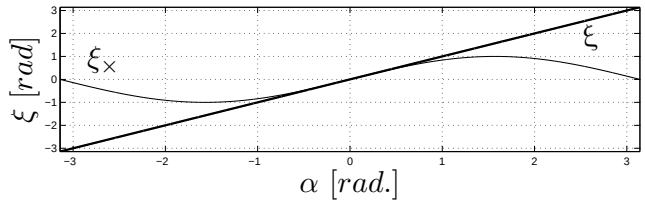

Fig. 4. Angular error estimation comparison, $\xi_\times \cong \sin(\alpha)$.

flux sensors or special machine). So, simulation results are provided to compare the actual stator flux with the estimated one.

A. Observer Sart-Up

This test shows the observer start–up behavior. The generation system is started first. At $t = 0.04\,s$ the observer starts estimating as shown in Fig. 5. The rotor speed is set to 0.6 p.u. and the rated stator electric load is fixed to 1 p.u.. The stator flux estimate converges to the actual value in less than $20\,ms$. This is clearly seen in Fig. 5 (a).

At the beginning, the rotor position estimation shows a very fast transient due to the PI convergence speed as can be seen on Fig. 5 (b). After that, the slow evolution is due to the stator flux convergence speed since a right rotor position estimation depends on correct estimation of stator flux.

B. Angular position estimation error rejection test

This test shows the rejection capabilities of the observer when a rotor position error is introduced. The observer has already converged to the actual values when the estimated rotor position is changed so ($e_\theta\,(0.15) = -\pi/2$) as can be seen on Fig. 6.

The angular error (e_θ) is defined as the difference between estimated rotor position ($\hat{\theta}_r$) and actual one ($e_\theta = \hat{\theta}_r - \theta_r$) while the rotor current angular error (ξ) is given by (15).

Fig. 6 (a) shows the angular error (e_θ) and the rotor current angular error (ξ) while Fig. 6 (b) shows the estimation errors of the stator flux dq–components. The rotor current angular error (ξ) reaches zero very fast although the angular error (e_θ) shows a very fast initial decrease but a small error remains until flux error reaches zero. This behavior can be explained as a cross coupling between the stator flux and rotor position estimation mechanisms. This is due to the selected gains of the proposed observer given by σ, K_{P_ω} and K_{I_ω}.

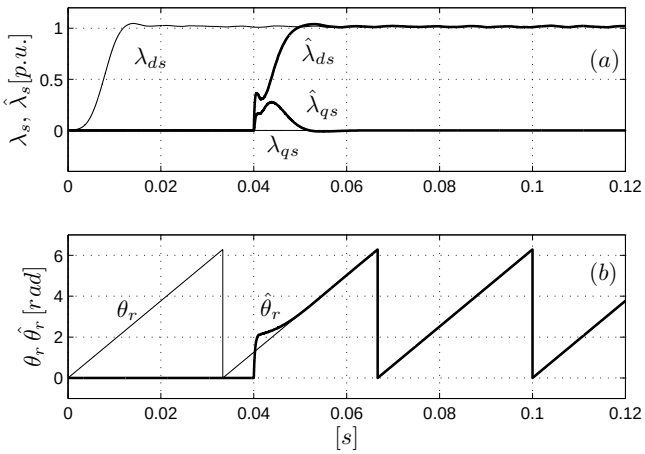

Fig. 5. Observer start–up simulation results (simulation test).

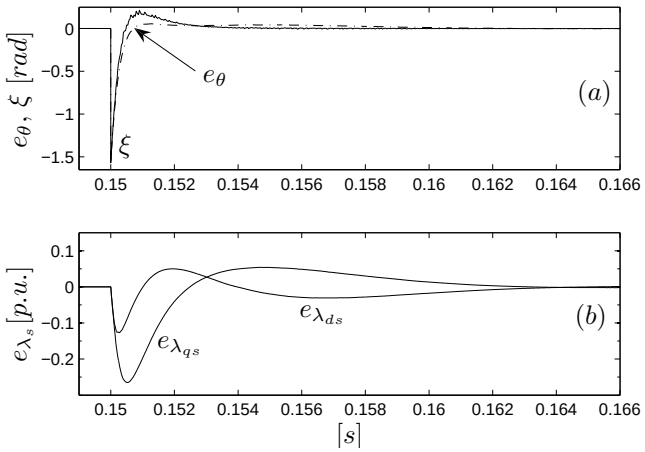

Fig. 6. Angular position estimation error rejection test (simulation test).

C. Estimated flux error rejection test

This test shows the rejection capabilities of the observer when stator flux dq–components errors are introduced as can be seen in Fig. 7. The observer has already converged to the actual values when the estimated stator flux dq–components are changed so that $e_{\lambda_{qs}} = 0.1$ p.u. and $e_{\lambda_{ds}} = -0.1$ p.u., at $t = 0.03\,s$.

Fig. 7 (a) shows the angular error (e_θ) and the rotor current angular error (ξ) while (b) shows the stator flux dq–components errors. The estimated flux error decays exponentially as stated on Section III-A reaching zero in less than $20\,ms$. The instantaneous change of the estimated stator flux components, provokes an instantaneous change of the rotor current angular error (ξ). Since the estimated rotor position is obtained as a result of a free–running integral, the angular error (e_θ) does not change instantaneously as shown in Fig. 7 (a). It is also shown that ξ reaches zero very fast but e_θ only reaches zero when the estimated stator flux converge to the actual value.

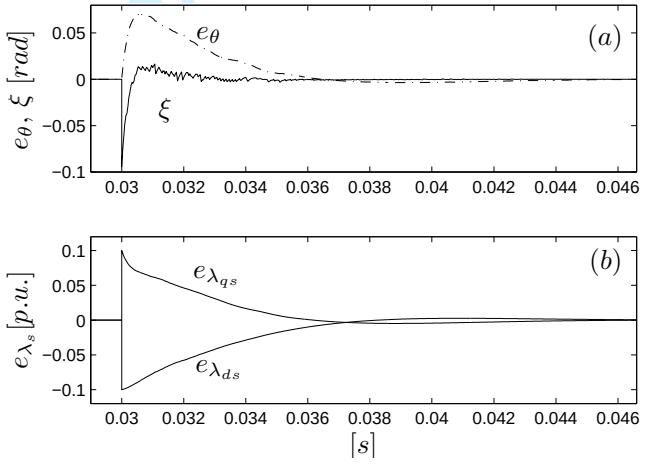

Fig. 7. Estimated flux error rejection test (simulation test).

Parameter mismatch should be considered when the whole control system performance is evaluated. The stator flux estimates depend on stator resistance r_s and stator inductance L_s. The stator resistance r_s varies with temperature which can change with load condition and rotor speed. A detailed analysis through simulation results can be found in [18].

V. Experimental Results

The performance of the proposed control system is evaluated through extensive experimental results covering a wide range of operating conditions. The test rig used to obtain the experimental results is shown on Fig. 8

The Rotor Converter (RC) is implemented using a bang-bang current control over a voltage source inverter to impose the DFIM rotor currents. In this work, the FEC shown on Fig. 1 is not implemented and the DC-Link voltage is achieved using a full bridge rectifier connected to machine stator terminals through a transformer. A dump resistive load is connected to DC-Link to burn the generated energy during super–synchronous speed operation. Stand-alone system requires initial energy for excitation. In this work a standard battery connected to the DC-Link through a diode is used to initialize the system, as can be seen on Fig. 8.

A capacitor bank, connected to the generator terminals ($C = 50\,\mu$F) is designed taking three premises into account: a) to filter the high frequency commutation noise induced by the RC, b) to smooth the voltage peak that appears after a sudden change of load on the generator terminals and c) to provide part of the magnetizing current reducing the current required by the rotor windings.

A purely resistive load was applied to the generator terminals. This load may be fixed in two values corresponding to 0.5 p.u. and 1 p.u. of the generator rated load.

The rotor speed is set using an adjustable speed drive (**ASD**). A standard PC is used to solve the observer and control equations. A National Instrument conversion board (NI-LAB-PC+) is used to acquire the signals obtained from current and voltage sensors. The machine parameters are listed on Table I. The gains of the PI controllers and the observer are listed on Table II.

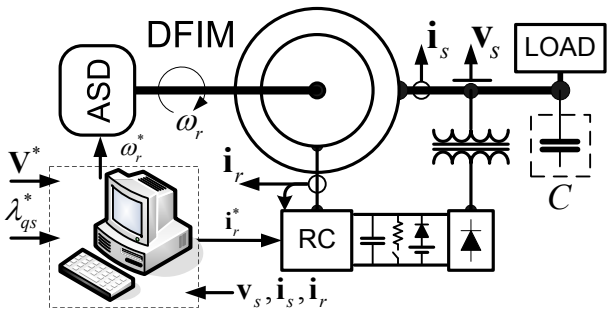

Fig. 8. Test rig used to obtain experimental results.

A. Load rejection capabilities

This test shows the system start–up and its behavior with load changes, while the DFIM rotor speed is set to 0.6 p.u.. The estimated stator flux and rotor position are used as feedback signals in control loops. The system is started with 1 p.u. of rated load connected on stator terminal. At $t = 0.118\,s$ the stator load is changed to 0.5 p.u. and at $t = 0.18\,s$ the load is set back to 1 p.u.. Fig. 9 shows the stator phase currents (a), the stator phase voltages (b), the stator voltage control loop error (c), the stator flux d and q–component (d) and the estimated rotor position error (e) along the whole test.

The stator voltage shows no significant perturbation considering the load change as can be seen on Fig. 10 (a) and (b). The control loop errors reaches zero in less than $40\,ms$. The control error dynamics depends on the control gains, the sampling time and the inverter switching frequency plus the load dynamics.

B. Speed rejection capabilities

This test shows the system speed change rejection capabilities. The generating system is working with 1 p.u. rated load

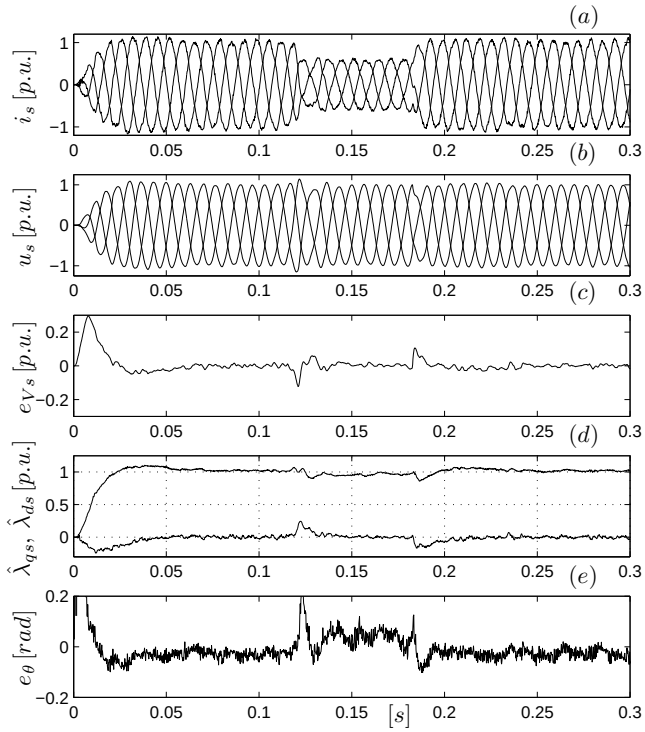

Fig. 9. Load change response.

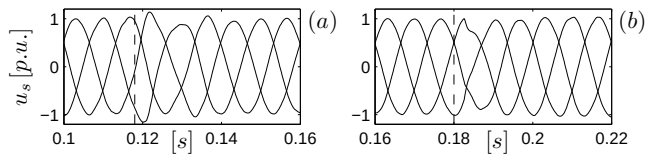

Fig. 10. Stator voltage during load change.

connected to stator terminals and the rotor speed is forced to follow the profile shown on Fig. 11 (e).

Speed changes are designed to evaluate the system on a very hard condition (acceleration $2400\ [rpm/s]$). The stator voltage magnitude control loop error is not affected by a speed change as can be seen on Fig. 11 (a) and (b). Frequency control loop error seen from from the variations of the flux q–components shown on Fig. 11 (c). It can be seen that there is no significant perturbation on d nor q–component during speed changes. Commutation noise mask the frequency and voltage control loop, and angular estimation errors as can be seen on Fig. 11 (b), (c) y (d). Even so, all errors remains at small values as can be seen from the presented results.

C. Steady State performance

This test shows the quality of the energy provided by the generation system using a rated load connected on stator terminal while the DFIM rotor speed is set to 0.6 p.u.. A stator phase voltage is plotted on Fig. 12 (a). It can be seen that stator voltage is a sinusoidal waveform with a small amount of 3^{rd} harmonic component in Fourier spectral decomposition as shown on Fig. 12 (b).

Stator voltage during speed variations is also shown in Fig. 13 (a). This stator voltage waveform is obtained from a zoom of Fig. 11 (a). In this case, stator voltage is very similar to that obtained at constant speed. This is easily verified by the Fourier spectrum shown in Fig. 13 (b).

VI. Conclusions

A sensorless control strategy for a DFIM working with variable–speed variable–load in stand alone power system was presented. An adaptive Luenberger observer is designed to estimate the stator flux and the rotor position of the DFIM. Experimental results have been presented to validate this proposal. These results have shown very good performance of the whole system even in presence of load and speed variations.

Moreover, this control strategy can be used successfully for synchronizing the generation system to connect it to the grid. Synchronism can be achieved aligning the stator flux reference frame with a fictitious grid flux vector obtained from grid voltages [21]. In this case, control loops should be changed to work properly controlling active and reactive power as required for grid connection [22]. The proposed flux observer can be used on either working condition with no further modifications.

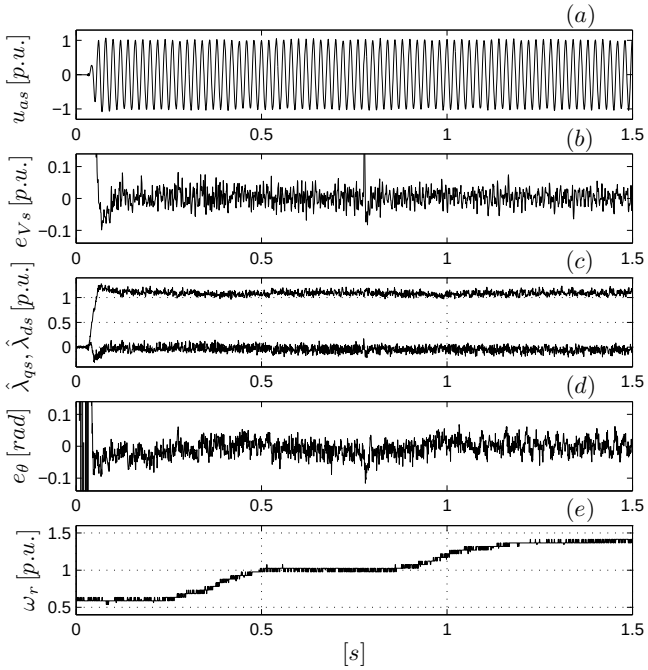

Fig. 11. System response during speed change.

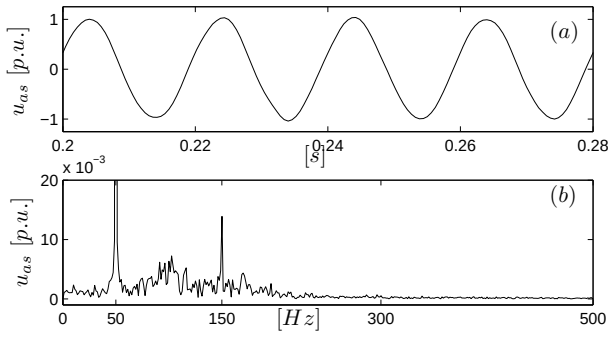

Fig. 12. Steady state stator voltage waveform during constant speed.

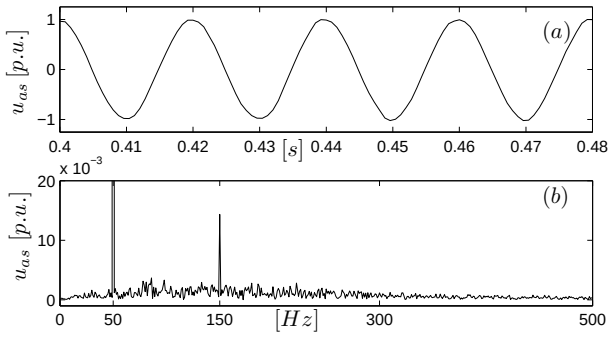

Fig. 13. Steady state stator voltage waveform during speed variations.

References

[1] A. C. Smith, R. Todd, M. Barnes, and P. J. Tavner, "Improved energy conversion for doubly fed wind generators," *IEEE Trans. on Ind. App.*, vol. 42, no. 6, pp. 1421 – 1428, Nov.-Dec. 2006.

TABLE I
Machine parameters (rated values)

Parameter	Value	Parameter	Value
P	$5.5\ [kW]$	ω_r	$1500\ [rpm]$
v_s	$220\ [V]$	L_s	$122.8\ [mH]$
i_s	$12\ [A]$	M	$121\ [mH]$
i_r	$16\ [A]$	r_s	$0.67\ [\Omega]$

TABLE II
CONTROLLER AND OBSERVER GAINS

Gain	Value	Gain	Value
K_{Pf}	7×10^2	K_{Pv}	0.1
K_{If}	2.8×10^5	K_{Iv}	10
$K_{P\omega}$	4×10^3	σ	-7×10^2
$K_{I\omega}$	4×10^6		

[2] J. Carrasco, L. Franquelo, J. Bialasiewicz, E. Galvan, R. Portillo-Guisado, M. Prats, J. Leon, and N. Moreno-Alfonso, "Power-electronic systems for the grid integration of renewable energy sources: A survey," *IEEE Trans. on Ind. Electron.*, vol. 53, no. 4, pp. 1002–1016, Aug. 2006.

[3] M. Aktarujjaman, M. Kashem, M. Negnevitsky, and G. Ledwich, "Control stabilisation of an islanded system with DFIG wind turbine," in *Proc. IEEE Int. Power and Energy Conf., (PECon'06).*, Nov. 2006, pp. 312 – 317.

[4] H. Polinder, F. Van der Pijl, G.-J. de Vilder, and P. Tavner, "Comparison of direct-drive and geared generator concepts for wind turbines," *IEEE Trans. on Energy Conv.*, vol. 21, no. 3, pp. 725 – 733, Sep. 2006.

[5] G. Iwanski and W. Koczara, "Sensorless direct voltage control of the stand-alone slip-ring induction generator," *IEEE Trans.on Ind. Electron.*, vol. 54, no. 2, pp. 1237 – 1239, Apr. 2007.

[6] A. Jain and V. Ranganathan, "Wound rotor induction generator with sensorless control and integrated active filter for feeding nonlinear loads in a stand-alone grid," *IEEE Trans. on Ind. Electron.*, vol. 55, no. 1, pp. 218 – 228, Jan. 2008.

[7] G. C. Verghese and S. R. Sanders, "Observers for flux estimation in induction machines," *IEEE Trans. on Ind. Electron.*, vol. 35, no. 1, pp. 85–94, Feb. 1988.

[8] C. Schauder, "Adaptive speed identification for vector control of induction motors without rotational transducers," in *Proc. IEEE IAS Annu. Meeting, 1989*, vol. 1, Oct. 1989, pp. 493 – 499.

[9] G. JinWen and W. XuHui, "Research on a novel motor flux observer based on voltaje model," in *Proc. 10th IEEE Int. Power Electron. Conf., (CIEP2006)*, Puebla, Mexico, Oct. 2006, pp. 1–5.

[10] R. Cardenas, R. Peña, J. Proboste, G. Asher, and J. Clare, "MRAS observer for sensorless control of standalone doubly fed induction generators," *IEEE Tran. Energy Conv.*, vol. 20, no. 4, pp. 710 – 718, Dec. 2005.

[11] R. Cárdenas, R. S. Peña, G. Asher, J. Clare, and J. Cartes, "MRAS observer for doubly fed induction machines," *IEEE Trans. on Energy Conv.*, vol. 19, no. 2, pp. 467– 468, Jun. 2004.

[12] R. S. Peña, R. Cardenas, J. Proboste, G. Asher, and J. Clare, "Sensorless control of a slip ring induction generator based on rotor current MRAS observer," in *Proc.* 36^{th} *IEEE Power Electron. Spec. Conf. (PESC05)*, Jun. 2005, pp. 2508–2513.

[13] R. Cardenas, R. Peña, J. Proboste, G. Asher, and J. Clare, "Rotor current based MRAS observer for doubly-fed induction machines," *IEEE Electron. Letters*, vol. 40, no. 12, pp. 769 – 770, Jun. 2004.

[14] H. Li, W. Xuhui, and C. Guilan, "General adaptive schemes for resistance and speed estiamtionin induction motor drives," in *Proc. 10th IEEE Conf. In Power Electron., COMPEL '06*, Jul. 2006, pp. 173–178.

[15] H. Li, W. Xuhui, and C. Guilan, "New general MRAS adaptive scheme to estimate stator and rotor resistance of induction motors," in *Proc. 41st IEEE IAS Annu. Meeting*, Oct. 2006, pp. 1775–1780.

[16] R. Bojoi, G. Griva, and F. Profumo, "Field oriented control of dual three-phase induction motor drives using a luenberger flux observer," in *Proc. 41st IEEE Ind. App. Conf. IAS'06*, 8-12 Oct. 2006, pp. 1253–1260.

[17] K. Ohyama, G. Asher, and M. Sumner, "Comparative analysis of experimental performance and stability of sensorless induction motor drives," *IEEE Tran. Ind. Electr.*, vol. 53, no. 1, pp. 178–186, Dec. 2005.

[18] D. Forchetti, G. O. Garcia, and M. I. Valla, "Sensorless control of Stand–Alone doubly fed induction generator with an adaptive observer," in *Proc. IEEE Int. Symp. On Ind. Electron. (ISIE2008)*, Cambridge UK, Jun.- Jul. 2008, pp. 2444–2449.

[19] P. C. Krause, O. Wasynczuk, and S. D. Sudhoff, *Analysis of Electric Machinery*, IEEE, Ed., 1996.

[20] D. Forchetti, J. A. Solsona, G. O. Garcia, and M. I. Valla, "A control strategy for stand-alone wound rotor induction machine," *Electric Power System Research (Elsevier)*, vol. 77, no. 2, pp. 163–169, Feb. 2007.

[21] R. S. Peña, R. Cardenas, J. Proboste, G. Asher, and J. Clare, "Sensorless control of doubly-fed induction generators using a rotor-current-based MRAS observer," *IEEE Trans. on Ind. Electron.*, vol. 55, no. 1, pp. 330 – 339, Jan. 2008.

[22] G. Iwanski and W. Koczara, "DFIG-based power generation system with UPS function for variable-speed applications," *IEEE Trans. on Ind. Electron.*, vol. 55, no. 8, pp. 3047 – 3054, Aug. 2008.